Highly Active, Durable Dispersed Iridium Nanocatalysts for PEM Water Electrolyzers

Shuai Zhao[a], Allison Stocks[a], Brian Rasimick[a], Karren More[b], and Hui Xu[a, *]

[a] Giner. Inc.

Newton, MA 02466

[b] Center for Nanophase Materials Sciences, Oak Ridge National Laboratory,

Oak Ridge, TN 37830

*Corresponding author. Tel.: +1 (781) 529-0573.

E-mail address: hxu@ginerinc.com (H. Xu).

Abstract

One of the primary challenges for proton exchange membrane (PEM) electrolyzers is the sluggish kinetics of the oxygen evolution reaction (OER) at the anode, which requires the use of precious metals or metal oxides, such as iridium (Ir) or iridium oxide (IrO_x), as the OER catalyst. This study introduces a one-pot surfactant-free polyol reduction method to disperse iridium nanoparticles on tungsten doped titanium oxide ($W_xTi_{1-x}O_2$) support. The polyol reduction approach for the Ir/$W_xTi_{1-x}O_2$ catalyst synthesis was systematically investigated to determine the influence of synthesis parameters on the catalysts' physical properties, and its electrochemical activity and durability. The most promising synthesized catalyst with 38 wt.% Ir ($Ir_{38\%}/W_xTi_{1-x}O_2$) demonstrated five times higher mass activity than an Ir-black baseline (the industry standard catalyst) based on rotating-disk electrode (RDE) studies. When tested in a real water electrolyzer system, the synthesized catalyst enabled the Ir loading to be lowered by an order of magnitude while retaining a similar electrolyzer performance found for the baseline Ir-black catalyst. The $Ir_{38\%}/W_xTi_{1-x}O_2$ catalyst also demonstrated remarkable stability, e.g., only small voltage (<20 mV) increase was observed during a 1200-hour durability test at a constant current density of 1500 mA/cm^2.

Key words: Proton exchange membrane; water electrolyzer; oxygen evolution reaction catalyst; iridium

1 Introduction

Proton-exchange membrane (PEM) water electrolyzers have been widely used for the production of highly pure hydrogen and oxygen for industrial, residential, and military applications. Most recently, PEM electrolysis has led to the wide adoption of power to gas (P2G) or power to mobile (P2M) when combined with renewable energy sources such as hydro, wind, and solar energies during off-peak periods [1, 2]. For the PEM water electrolysis, the anodic oxygen evolution reaction (OER) requires a much higher overpotential compared to its cathodic hydrogen evolution reaction (HER) [3, 4]. Iridium (Ir) or iridium oxide (IrO_x) are the most widely used catalysts for the OER due to a combination of high activity and durability [5-7]. However, large-scale implementation and commercialization of PEM electrolyzers currently require substantial amounts of Ir, which is both scarce and expensive. Therefore, improving the activity of Ir-based catalysts to lower the catalyst loading is a priority for the wide-scale implementation of affordable electrolysis systems.

Significant research efforts have been undertaken to disperse precious metal nanoparticles on chemically stable supports with high surface areas to improve their mass activities; however, unlike supported Pt electrocatalysts for the oxygen reduction reaction (ORR) in fuel cells [8-13], which has been extensively studied, research into the synthesis of supported Ir catalysts is much less reported in the literature. A significant difference between the support materials traditionally used for Pt for the ORR and those used for Ir for the OER is the high electrochemical stability or oxidation resistance required for the OER catalyst support, which strictly limits the use of carbon black support for the OER catalyst, as illustrated in **Fig. 1**. The surfaces of carbon black particles can be

electrochemically oxidized at potentials above 0.207 V vs. normal hydrogen electrode (NHE), as shown in **Equation 1** [14, 15]:

$$C + 2H_2O \rightarrow CO_2(g) + 4H^+ + 4e^-,\ E^\circ = 0.207\ V \qquad \textbf{(Equation 1)}$$

Thus, carbon black supports are intrinsically unstable even under normal fuel cell operating conditions, which has raised some concerns for long-term application for PEM fuel cells [16]. In the highly oxidizing environment of PEM electrolyzers, oxidation/corrosion of the carbon support may occur rapidly, which then leads to the collapse of the catalyst layer porous structure, affects the electrical conduction in the catalyst layer, and can affect water management.

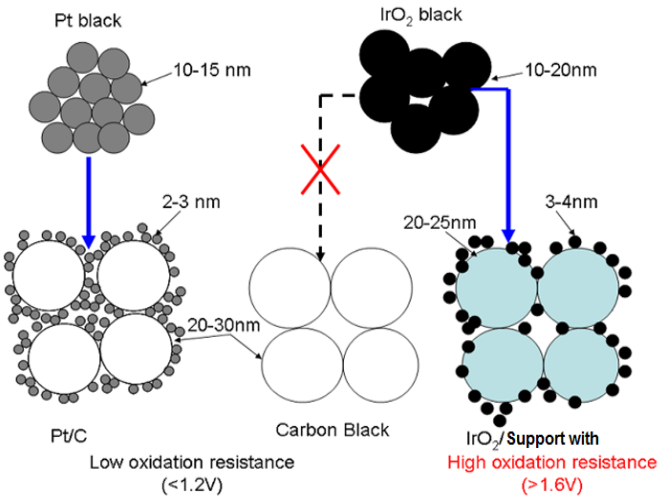

Figure 1. Schematic of catalyst support comparison for ORR in fuel cells and OER in electrolysis cells.

Therefore, rather than using carbon black support materials, various conductive or semi-conductive metal oxides such as modified titanium oxide, niobium oxide, tin oxide, and antimony-doped tin oxide (ATO), have been investigated as possible support candidates for OER catalysts in PEM electrolyzer applications to (1) decrease the overall catalyst loading and cost of the catalyst or (2) manipulate and control the dispersion of Ir

to improve the catalyst activity and durability [9, 17-19]. This combined strategy can serve to stabilize the initial catalyst surface area and also significantly improve the mass activity of the catalysts. Many supported OER catalysts achieve a high initial OER mass activity due to an increase in the Ir nanoparticle surface area. However, a more critical challenge is establishing the long-term durability of supported Ir electrocatalyst during real PEM electrolysis operation, which has been largely neglected. Most of the data reported in the literature has focused on rotating-disk electrode (RDE) results with chronopotentiometry curves acquired at a current density as low as 10 mA/cm^2, rather than reporting performance and durability data for a full electrolysis cell.

In this study, we introduce a template-free and surfactant-free polyol reduction method to deposit Ir nanoparticles onto tungsten-doped titanium oxide ($W_xTi_{1-x}O_2$) particle supports, due to the excellent stability exhibited by $W_xTi_{1-x}O_2$ in strongly oxidizing environments. The deposited Ir was systematically investigated in the polyol reduction reaction in terms of the influence of different synthesis parameters on the resultant Ir particle size and distribution on the $W_xTi_{1-x}O_2$ support particles. These physical properties were correlated to the catalyst's electrochemical properties measured by both RDE and in operating electrolyzer cells. The synthesized catalyst with 38 wt.% Ir ($Ir_{38\%}/W_xTi_{1-x}O_2$) demonstrated a five times higher mass activity than the industrial standard Ir-black baseline, based on RDE studies. When tested in a PEM water electrolyzer cell, this same catalyst enabled the Ir loading to be lowered by an order of magnitude ($0.3mg_{Ir}/cm^2$) while it retained a similar electrolyzer performance as the baseline Ir-black ($3mg_{Ir}/cm^2$). Long-term durability test (up to 1200 hours) of the selected catalyst $Ir_{38\%}/W\text{-}TiO_2$ in the electrolysis cell exhibited less than 20 mV performance decay at a current density of 1500 mA/cm^2.

2 Experimental Section

2.1 Synthesis of Iridium/Iridium-Oxide Catalysts Supported on Tungsten-doped Titanium Oxide through Template- and Surfactant- free Polyol Reduction

Typically, 1.2 g of sodium hydroxide pellets were ground and dissolved into 150 ml ethylene glycol to produce a 0.2 M NaOH solution under continuous stirring overnight. 0.7 g of a commercially available tungsten-doped titanium oxide ($W_xTi_{1-x}O_2$) support (*c.a.* 30 nm in diameter) was added and the solution was sonicated while being stirred for 45 minutes. Then, 0.7 g of the metal precursor ($IrCl_3.xH_2O$) was added to the solution and stirred for three hours. A homogeneously dispersed, caramel-yellow colored, liquid mixture was obtained, which was heated to 175°C on a hot plate and reacted for three hours. The resulting mixture was cooled naturally to room temperature and then mixed into 1.5 L of deionized (DI) water. During mixing, nitric acid was slowly added until the pH of the solution was approximately 1~2. The solution was then stirred for three additional hours. After Ir precipitation, the Ir/$W_xTi_{1-x}O_2$ particles were separated and washed through centrifugation three times until clear supernatant was obtained. The collected Ir/$W_xTi_{1-x}O_2$ nanoparticles were dried in a vacuum oven at 110°C for four hours. Several synthesis parameters, such as the precursor to support ratio, initial pH value, and reaction temperature, were varied to manipulate the Ir catalyst nanoparticle size and distribution on the $W_xTi_{1-x}O_2$ support particles, as discussed in Section 3.2.

2.2 Physical Characterizations

The crystal structure of the Ir-based electrocatalysts were evaluated by using a Bruker D8 Advance X-ray diffractometer (XRD) with a Cu $K\alpha_1$ ceramic X-ray tube (λ= 0.1540562 nm) and a LynxEye Super Speed detector. The diffraction angle (2θ) was varied

from 5° to 90° at a scan rate of 0.0285°/second. The bulk elemental composition of the supported Ir catalysts were determined by energy dispersive X-ray spectroscopy (EDS) fully integrated in a Phenom ProX desktop scanning electron microscope (SEM) equipped with a field emission source. Images were captured using a backscatter electron detector with the SEM operated at an accelerating voltage of 15 kV. The microstructure of the $Ir/W_xTi_{1-x}O_2$ and Ir particle sizes were investigated by transmission electron microscopy (TEM) using an FEI Tecnai T12 and by high-resolution TEM using a JEOL JEM-2010 (instruments located at the Institute of Materials Sciences, University of Connecticut). Samples for TEM were prepared by ultrasonically dispersing particles in ethanol and dispersing the solution on 3mm holey carbon-coated copper grids. Pre- and post-test membrane electrode assemblies (MEAs) and changes in catalyst distributions were studied by scanning transmission electron microscopy (STEM). Samples for STEM were prepared by diamond knife microtomy (Leica UCT). High angle annular dark field (HAADF) STEM imaging and high-resolution with EDS mapping were conducted using a JEOL JEM-2200F aberration-corrected STEM (instrument located at Oak Ridge National Laboratory).

2.3 Electrochemical Characterization in Rotating Disk Electrode (RDE) System

Electrochemical experiments were carried out in a three-electrode electrochemical cell with a water jacket. A Pt wire and a $Hg/HgSO_4$ electrode (Pine Research Instruments) were used as the counter and reference electrodes, respectively. Polarization curves for the OER were recorded using a VersaSTAT 3 potentiostat (Princeton Applied Research). The electrolyte used in the electrochemical tests was 0.1 M perchloric acid ($HClO_4$) solution prepared from 1 M perchloric acid (≥85.0% Sigma-Aldrich). All the polarization curves

for activity comparisons and the intermediate curves for durability tests were collected at a scan rate of 5 mV/s and electrode rotation rate of 1600 rpm. The reference electrode was converted to reversible hydrogen electrode (RHE) by calibrating the $Hg/HgSO_4$ electrode with hydrogen reference electrode (eDAQ, ET070 Hydroflex™ Hydrogen Reference Electrode) before each experiment. Preparation for the working electrode was to disperse the electrocatalyst onto a mirror-polished 5 mm-diameter Au electrode (Pine Research Instrumentation). The Au electrode was polished to a mirror finish using a 0.05 μm alumina-particle suspension (Buehler) on a moistened polishing microcloth (Buehler) and washed ultrasonically with ultra-pure 18.2 MΩ DI water (from a Millipore Direct-Q 3UV purification system) for 4 minutes prior to each experiment. The catalyst ink dispersion was prepared (2 mg catalyst: 0.3 mL isopropanol: 0.7 mL DI water: 8 μL 5 wt% Nafion solution) by sonication for 20 minutes, forming a uniform suspension. 8 μl of the suspension was added dropwise onto the Au electrode with a micropipet and then dried in air for 60 minutes on an inverted RDE at 300 rpm (Pine Research Instrumentation). A homogeneous black thin film was obtained on top of the Au electrode. The loading of catalyst on the working electrode was approximately 16 $\mu g/cm^2$.

2.4 Electrochemical Characterizations in PEM Electrolyzers

Full cell operation was conducted at 80°C, in ambient pressure, and a liquid water feed to the anode. The cell hardware was standard Fuel Cell Technologies 50 cm^2 hardware, except the anode flow field was Pt-plated Ti rather than graphite. MEAs were fabricated by hot-pressing catalyst decals onto a Nafion$^@$ 115 membrane (at 185 °C and 6 MPa for 15 min). For all cell testing, the cathode catalyst was Pt/C at a loading of 0.4 mg_{Pt}/cm^2. Several experimental anode catalysts were evaluated and compared with a

'standard' anode made using a blend of 2 mg/cm^2 Ir-black and 2 mg/cm^2 Pt-black. The cell resistance was measured *in situ* using a simplified version of electrochemical impedance spectroscopy analysis known as high-frequency resistance (HFR). For this technique, the operating current of the cell was rapidly pulsed at 1 kHz to 10% above the baseline current. The resulting pulsation in voltage was related to the pulsation in current and used to calculate the real component of the cell impedance. For durability testing, the cells were operated at a current density at 1.5 A/cm^2.

3 Results and Discussion

3.1 Down-Selection of Support Materials

Table 1. Conductivity and electrochemical stability of different support candidates for Ir/IrO_x oxide for OER catalyst in PEM electrolyzers.

Material	Conductivity	Electrochemical Stability
Titanium Carbide	**High**	Poor
ITO (90% In_2O_3: 10% SnO_2)	**High**	Poor
Titanium Nitride	**Medium**	Poor
W-doped TiO_2 ($W_xTi_{1-x}O_2$)	**Medium**	**Good**
TiO_2 Nanowire	Low	**Good**

The two most critical properties for a support material for Ir/IrO_x for use as an OER catalyst for PEM electrolyzers are conductivity and electrochemical stability under a strong acidic environment and an oxidizing voltage as high as 2 V. A few support candidates that have been intensely studied [13, 17, 20-22] are listed in **Table 1** with their corresponding properties and levels rated as follows: conductivity: high (>0.1 S-cm^{-1}), medium (0.001-0.1 S-cm^{-1}) and low (<0.001 S-cm^{-1}); electrochemical stability: poor (surviving < 5000

cycles, from 1.2 V to 2 V in acid) and good (surviving > 10,000 cycles, from 1.2 V to 2 V in acid). Only the titanium oxide based support (TiO_2 nanowires) survives under harsh oxidizing and acidic environment, but exhibits a low conductivity. However, surface and bulk doping of TiO_2 structures have been used successfully to alter the ionic/electrical conductivity of TiO_2 by introducing intrinsic vacancies into the crystalline structure. For example, W/Nb substitutional-doping and V/Fe interstitial-doping in TiO_2 can create anion vacancies that improve the conductivity [23-25].

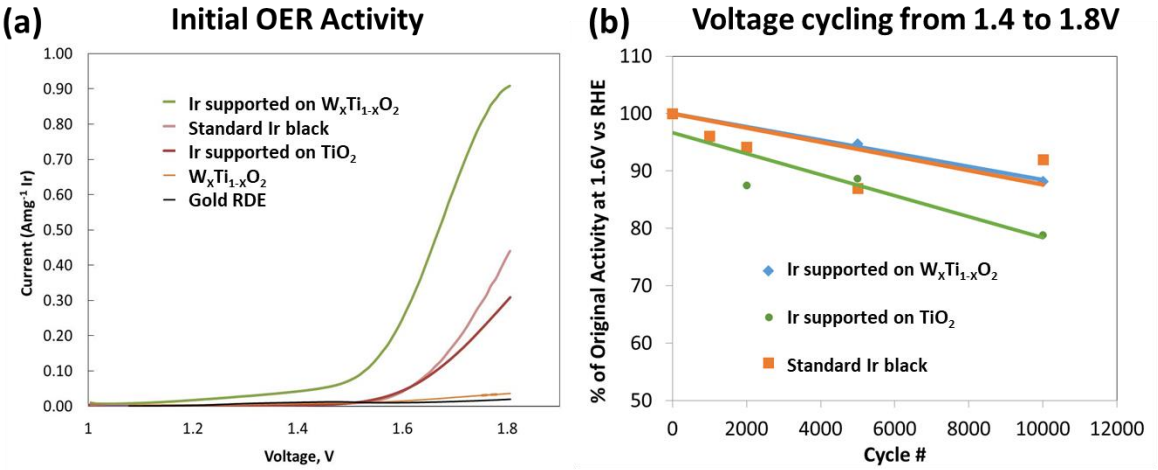

Figure 2. (a) OER activity comparing different supported Ir catalysts and raw support materials; (b) catalyst durability for commercial Ir-black and supported Ir catalysts.

Based on the results shown in Table 1, Ir was supported on tungsten-doped TiO_2 ($Ir/W_xTi_{1-x}O_2$) for evaluating the OER activity using RDE, the results of which are shown in **Fig. 2a**. For comparison, Au (RDE baseline), $W_xTi_{1-x}O_2$ without Ir, commercial Ir-black, and Ir supported on TiO_2 (Ir/TiO_2) were also evaluated and are also shown in **Fig. 2a**. The $Ir/W_xTi_{1-x}O_2$ catalyst showed the lowest onset potential for OER and highest current density at a fixed voltage of 1.6 V, even compared to the commercial Ir-black catalyst; the catalyst activity (defined as current density @ 1.6 V) was improved from 0.05 $A\text{-}mg^{-1}_{Ir}$ for

the Ir-black to 0.25 A-mg$^{-1}_{Ir}$ for the Ir/$W_xTi_{1-x}O_2$ catalyst, a five-fold increase. However, Ir/TiO_2 showed an inferior current density compared to standard Ir-black due to the low electrical conductivity of the TiO_2 support material. The Au baseline and support only, $W_xTi_{1-x}O_2$, barely exhibited any OER activity. Furthermore, the durability of the two supported Ir catalysts, Ir/$W_xTi_{1-x}O_2$ and Ir/TiO_2, were compared with standard Ir-black using RDE cycling from 1.4 V to 1.8 V at a scan rate of 500 mV/s in 0.1 M perchloric acid. The current densities at 1.6 V were recorded after different numbers of cycles and converted to percentages of original activity (**Fig. 2b**). The activity of the Ir/$W_xTi_{1-x}O_2$ catalyst remained *ca*. 90% of the original current density after 10,000 cycles, which was comparable to that for the standard Ir-black catalyst, while the Ir supported on TiO_2 only retained 80% of the original activity. Based on these preliminary RDE results, Ir/$W_xTi_{1-x}O_2$ was selected as the support for further study.

3.2 Synthesis-Property Relationship Analysis

The physical properties of the as-synthesized Ir/$W_xTi_{1-x}O_2$ catalyst produced using the procedure [26, 27] provided in Section 2.1 were further investigated. The crystal structure and phases present in the Ir/$W_xTi_{1-x}O_2$ were evaluated by XRD, as shown in **Fig. 3**. The Ir-black exhibited the standard face-centered-cubic crystallographic peaks of (111), (200), (220), (311), and (222) for 2θ between 20°-90°, and these XRD data were used as a baseline for evaluating the XRD data acquired from the Ir/$W_xTi_{1-x}O_2$. The corresponding Ir peaks for the Ir/$W_xTi_{1-x}O_2$ showed metallic Ir formed on the $W_xTi_{1-x}O_2$ support surfaces, consistent with data obtained for Ir-black except with much broader peak widths due to the smaller size of the Ir nanoparticles on $W_xTi_{1-x}O_2$. Other than the major peaks observed for Ir, the Ir/$W_xTi_{1-x}O_2$ also exhibited (211) and (002) peaks that corresponded to the support

and were consistent with the rutile phase/structure of TiO_2. EDS was used to determine the average Ir wt.% on the different catalyst samples, which are labelled as $Ir_{25\%}/W_xTi_{1-x}O_2$, $Ir_{28\%}/W_xTi_{1-x}O_2$, $Ir_{38\%}/W_xTi_{1-x}O_2$, $Ir_{73\%}/W_xTi_{1-x}O_2$, $Ir_{87\%}/W_xTi_{1-x}O_2$.

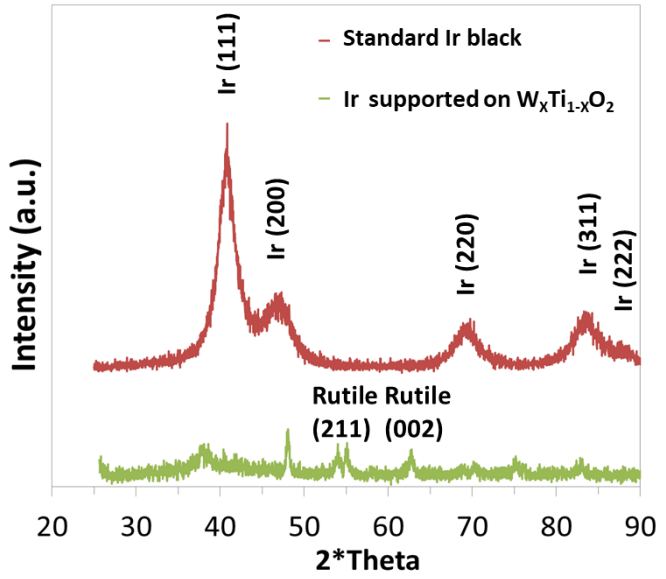

Figure 3. XRD pattern for Ir-black and $Ir/W_xTi_{1-x}O_2$.

The catalyst synthesis parameters were varied to study the relationship between physical properties and electrochemical performance of the $Ir/ W_xTi_{1-x}O_2$ catalyst. The Ir particle size and distribution can be tuned by manipulating key parameters, such as pH of the solution, reaction temperature, and Ir loading. For the template- and surfactant- free polyol reduction of precious metal, Ir^{3+} ions were reduced to metallic Ir with the oxidation of ethylene glycol to aldehydes, followed by oxidation of glycolic and oxalic acid, and finally to CO_2 or carbonate when OH^- groups of ethylene glycol interact with Ir^{3+} ion sites. During the reaction process, the glycolate anions formed in the presence of NaOH act as good stabilizers for Ir colloids, possibly forming chelate-type complexes via its carboxyl groups that prevent agglomeration of the Ir particles on the support [28, 29]. This was followed by the addition of dilute acid to separate and redisperse the Ir particles without

changing their size [30]. Lowering the initial pH of the solution may cause more Ir nanoparticle agglomeration and growth, as evidenced by the TEM images comparing $Ir_{28\%}/W_xTi_{1-x}O_2$ (formed using 0.03 M NaOH) in **Fig. 4b** with $Ir_{25\%}/W_xTi_{1-x}O_2$ (formed using 0.2 M NaOH) in **Fig. 4a**. The Ir particle size increased to about 3-4 nm and Ir nanoparticles became more agglomerated using 0.2 M NaOH.

It is also well known that the reaction temperature influences the final Ir particle size, e.g., higher temperature reactions produce smaller particle sizes due to the much faster Ir nuclei formation rate than the Ir particle growth rate; at lower temperatures, the formation of Ir nuclei is more difficult, thus, newly reduced Ir grows on existing Ir nuclei and yields larger particles [26]. Higher Ir loadings can also lead to larger particles due to the abundance of reduced Ir and agglomeration of nanoparticles. The TEM images of $Ir_{73\%}/W_xTi_{1-x}O_2$ and $Ir_{87\%}/W_xTi_{1-x}O_2$ in **Figs. 4c** and **4d** directly proved this with the average particle size increased to around 5-6 nm.

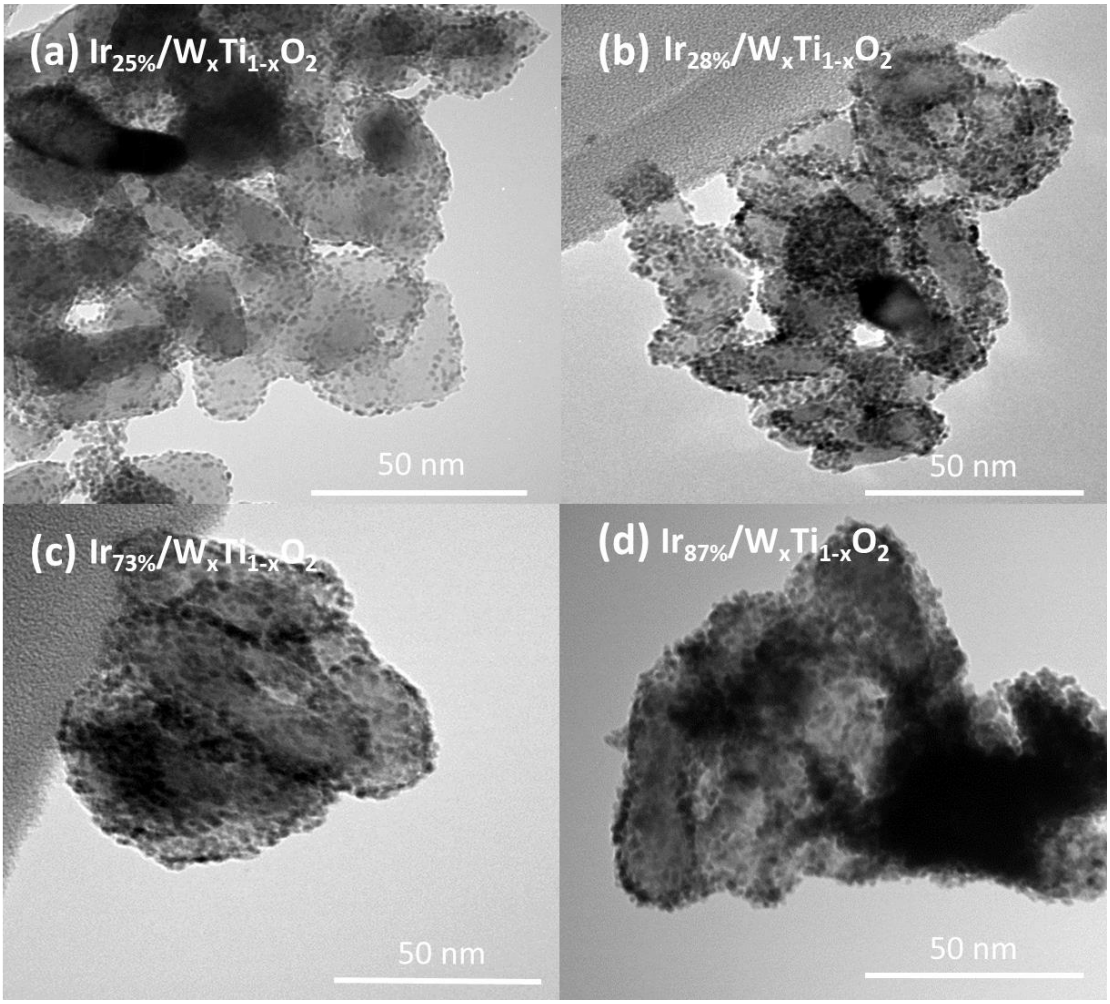

Figure 4. TEM images of Ir nanoparticles supported on $W_xTi_{1-x}O_2$ resulting from different synthesis procedures: (a) $Ir_{25\%}/W_xTi_{1-x}O_2$; (b) $Ir_{28\%}/W_xTi_{1-x}O_2$; (c) $Ir_{73\%}/W_xTi_{1-x}O_2$; (d) $Ir_{87\%}/W_xTi_{1-x}O_2$.

The Ir loadings for samples shown in **Fig. 4** ranged from ~25wt.%-87 wt.% (**Fig. 4a-d**); however, $Ir/W_xTi_{1-x}O_2$ prepared with a medium Ir loading of 38 wt.% was also synthesized. **Fig. 5** shows HAADF-STEM images (**5a, 5c**) and corresponding EDS elemental maps (**5b, 5d**) of the $Ir_{38\%}/W_xTi_{1-x}O_2$ catalyst. HAADF-STEM imaging is commonly referred to as *Z*-contrast imaging, where the contrast displayed in the image scales as a function of the atomic number squared, Z^2; e.g., heavier elements image brighter

(Ir nanoparticles will image brightly) and lighter elements exhibit less contrast (the W-doped TiO_2 support particles appear darker in the image). The HAADF-STEM image presented in **Fig. 5c** shows the typical morphology of the $Ir_{38\%}/W_xTi_{1-x}O_2$; a network of linked Ir nanoparticles forms on the surface of a single ~30 nm $W_xTi_{1-x}O_2$ support particle. Most of the $W_xTi_{1-x}O_2$ particles are thin plates and exhibit a "bean-shaped" or elongated geometry, and the Ir nanoparticles tend to be somewhat aggregated rather than highly dispersed on the surface. The corresponding EDS maps show clearly that the Ir does not form a continuous coating on the surface of the $W_xTi_{1-x}O_2$ particles, but forms as a "lacey" or "chain-like" network of interconnected nanoparticles on the surface of $W_xTi_{1-x}O_2$. The formation of conductive Ir chain can facilitate electron transfer between the active Ir particles on the surface of the electrode, even if the support does not possess sufficient conductivity. A higher magnification HAADF-STEM image of an Ir chain region is shown in **Fig. 5e**; the lattice spacing within individual nanoparticles (see green circle) confirms the formation of metallic Ir nanoparticles that are linked together forming a chain or island of Ir nanoparticles. There are also isolated single Ir atoms scattered/dispersed across the $W_xTi_{1-x}O_2$ surface between the inter-connected chain-like networks of Ir nanoparticles.

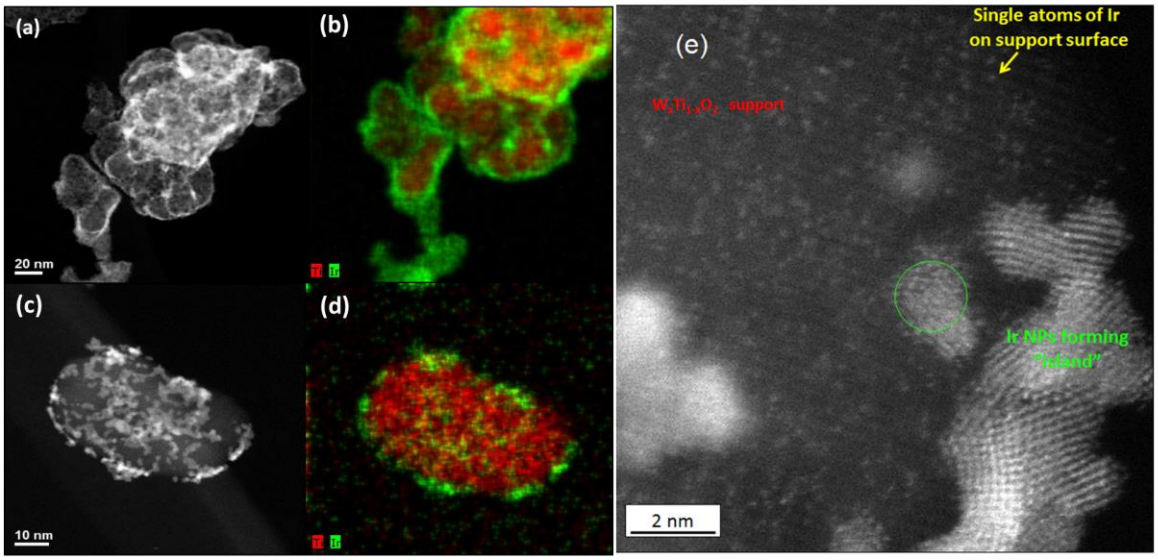

Figure 5. (a) (c) HAADF-STEM images and (b) (d) corresponding EDS elemental map of $Ir_{38\%}/W\text{-}TiO_2$ (Ti=red; Ir=green); (e) Atomic-resolution HAADF-STEM image showing interlinked chain/island of Ir nanoparticles with dispersed single atoms of Ir (bright dots designated by yellow arrow) on the surface of the $W_xTi_{1-x}O_2$ support particle (darker background).

3.3 Activity in RDE Studies

$Ir/W_xTi_{1-x}O_2$ samples with different Ir loadings and Ir particle sizes were RDE tested for OER activity. The OER linear sweep curves in **Fig. 6a** were collected at a scan rate of 5 mV/s at 1600 rpm in 0.1 M $HClO_4$. All samples exhibited similar onset potentials for the OER, but the current density at fixed voltages followed the trend of $Ir_{25\%}/W_xTi_{1-x}O_2$ > $Ir_{28\%}/W_xTi_{1-x}O_2$ > $Ir_{38\%}/W_xTi_{1-x}O_2$ > $Ir_{87\%}/W_xTi_{1-x}O_2$ > $Ir_{73\%}/W_xTi_{1-x}O_2$ > standard Ir-black. This current density trend is correlated to the trend of Ir particle size, which becomes smaller as the Ir loading on the $W_xTi_{1-x}O_2$ support decreases. However, for the catalysts with 73% and 87% Ir loading, the current density increased only slightly compared to the baseline Ir-black, likely due to the much larger Ir agglomerates that formed

at these higher Ir loadings. The performance was significantly improved when the Ir loading was lowered to 38%, where a better Ir dispersion and smaller Ir particle sizes were observed. To better compare the catalysts with different Ir loadings, the current densities at 1.5 V and at 1.8 V were measured, where the lower voltage represents intrinsic kinetic activity while the higher voltage represents the ohmic and transport losses. These two current densities vs. the Ir loading are plotted in **Fig. 6b**; for $Ir/W_xTi_{1-x}O_2$ with an Ir loading at lower than 38%, the intrinsic kinetic activity was clearly better than that of the catalysts with higher Ir loadings or for Ir-black. A higher current density was also observed at the higher voltage (1.8 V) on catalysts with medium or low Ir loadings, which is likely due to greater access to the active surface area of much smaller Ir particles and less Ir nanoparticle agglomeration. The durability of the $Ir/W_xTi_{1-x}O_2$ catalysts with different Ir loadings was also screened by RDE. $Ir_{38\%}/W_xTi_{1-x}O_2$ showed the best durability among all the catalysts, which may be due to the unique chain-like network formed by the Ir nanoparticles. Cycling in RDE was from 1.4 V to 1.8 V at a scan rate of 500 mV/s in 0.1 M perchloric acid. The current density at 1.6 V retained *ca*. 90% of the original current density after 10,000 cycles for $Ir_{38\%}/W_xTi_{1-x}O_2$ (**Fig. 6c**).

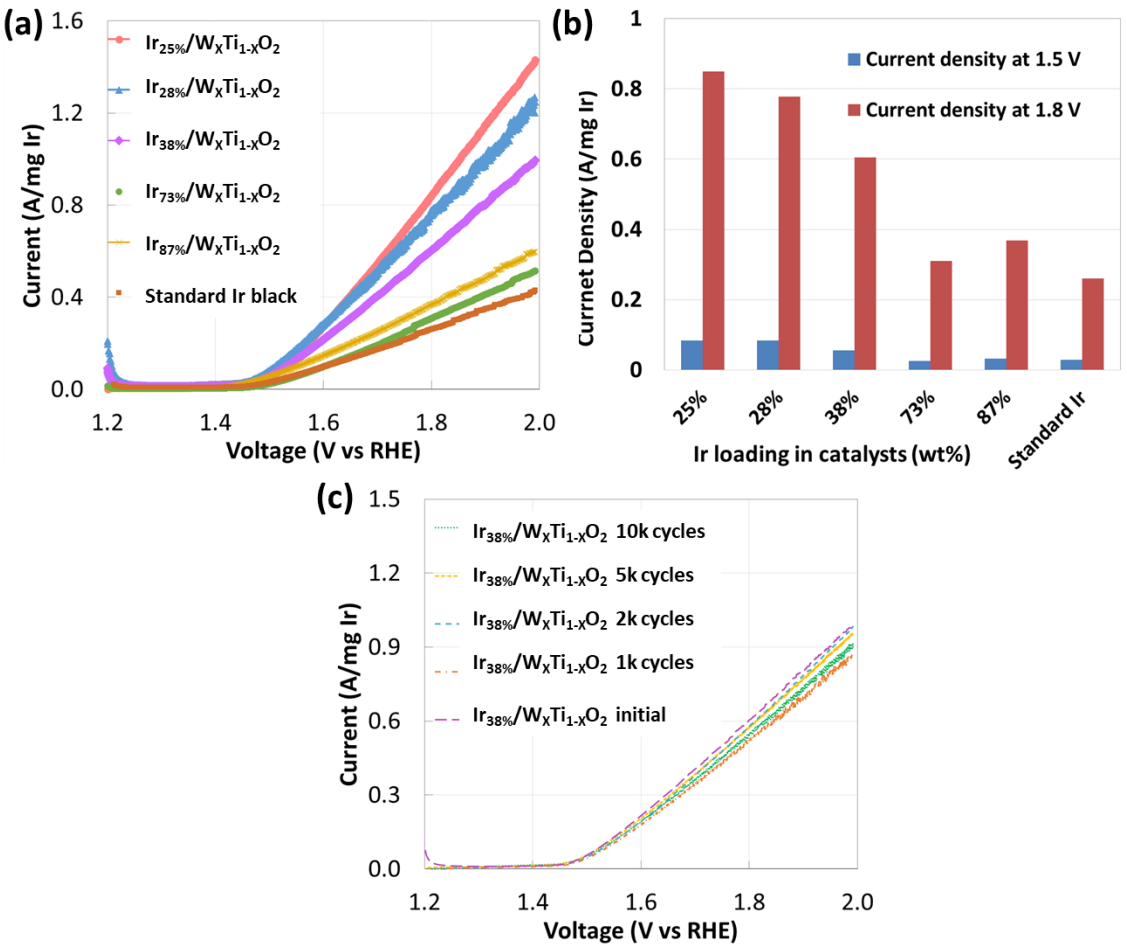

Figure 6. (a) OER activity comparison in RDE setup; (b) current density comparison at 1.5 V and 1.8 V of $Ir_{25\%}/W_xTi_{1-x}O_2$, $Ir_{28\%}/W_xTi_{1-x}O_2$, $Ir_{38\%}/W_xTi_{1-x}O_2$, $Ir_{73\%}/W_xTi_{1-x}O_2$, $Ir_{87\%}/W_xTi_{1-x}O_2$, and Ir-black; (c) durability test of $Ir_{38\%}/W_xTi_{1-x}O_2$ in RDE by cycling voltage from 1.4 to 2.0 V at 500 mV/s at room temperature.

3.4 MEA Test

The catalysts with different Ir loadings were integrated with a Nafion 115 membrane and gas diffusion media to fabricate MEAs. The MEA performance was compared in an operating electrolyzer single cell against the performance of the standard Ir-black used as a baseline, the results of which are shown in the polarization curves in **Fig. 7a**. The HFR for $Ir_{25\%}/W_xTi_{1-x}O_2$, $Ir_{38\%}/W_xTi_{1-x}O_2$, $Ir_{73\%}/W_xTi_{1-x}O_2$, $Ir_{87\%}/W_xTi_{1-x}O_2$ and

Ir-black are 0.118 Ohm-cm^2, 0.115 Ohm-cm^2, 0.205 Ohm-cm^2, 0.16 Ohm-cm^2, and 0.11 Ohm-cm^2, respectively. Only $Ir_{38\%}/W_xTi_{1-x}O_2$ (the medium Ir loading) demonstrates better activity than Ir-black, unlike the RDE measurements where all catalysts showed a higher activity than Ir-black. The catalytic performance difference between RDE and MEA is mainly reflected by the HFR value since the internal resistance-corrected (IR-Corrected) curves (**Fig. 7b**) manifest a similar trend after accounting for the resistance factor. The higher HFR for $Ir_{25\%}/W_xTi_{1-x}O_2$, $Ir_{73\%}/W_xTi_{1-x}O_2$, and $Ir_{87\%}/W_xTi_{1-x}O_2$ compared to the HFR for $Ir_{38\%}/W_xTi_{1-x}O_2$ may be due to the higher interfacial resistance of the former resulting from more exposure of the support material $W_xTi_{1-x}O_2$ due to aggregation and migration of Ir during decal transfer. This morphology change occurs in the samples with low Ir loadings due to less coverage across the support material surfaces, as well as those samples with higher Ir loadings since there is so much Ir nanoparticle aggregation. Only the $Ir_{38\%}/W_xTi_{1-x}O_2$ catalyst with medium Ir loading retained better activity than the Ir-black baseline in both RDE and an operating electrolyzer, indicating only slight morphological changes occur in this catalyst structure during MEA fabrication process.

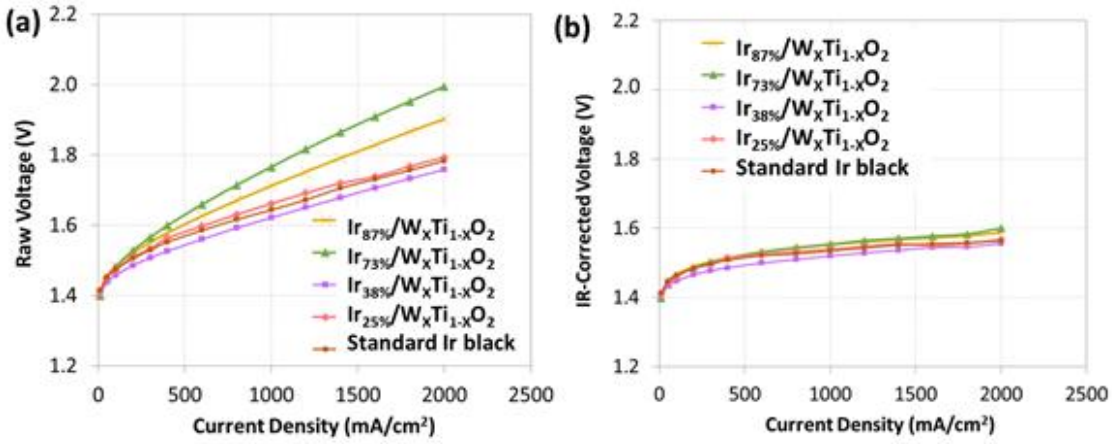

Figure 7. (a) Single cell MEA performance in electrolyzers (raw voltage) and (b) IR-corrected polarization curves for $Ir_{25\%}/W\text{-}TiO_2$ (pink), $Ir_{28\%}/W\text{-}TiO_2$ (blue), $Ir_{38\%}/W\text{-}TiO_2$

(purple), $Ir_{73\%}/W\text{-}TiO_2$ (green), $Ir_{87\%}/W\text{-}TiO_2$ (yellow) (0.4 mg_{Ir}/cm^2), and standard Ir-black (2 mg_{Pt}/cm^2+2 mg_{Ir}/cm^2) with Pt/C cathode (0.4 mg_{Pt}/cm^2) at 80 °C.

To further assess the performance of the $Ir/W_xTi_{1-x}O_2$ catalyst, we tested the MEA with $Ir_{38\%}/W_xTi_{1-x}O_2$ (Ir loading 0.4 mg/cm^2) directly with the commercial Ir-black (Ir loading 0.4 mg/cm^2) and a Giner standard MEA (2 mg_{Pt}/cm^2 + 2 mg_{Ir}/cm^2), the results of which are compared in **Fig. 8**. $Ir_{38\%}/W_xTi_{1-x}O_2$ exhibits outstanding performance in a full-cell PEM electrolyzer. At 0.4 mg/cm^2 Ir loading, it nearly matches the performance of the Giner standard anode (2 mg_{Pt}/cm^2 + 2 mg_{Ir}/cm^2) while reducing the Ir loading by a factor of five and the precious metal loading by a factor of 10. In a comparison with 0.4mg/cm^2 Ir-black, $Ir_{38\%}/W_xTi_{1-x}O_2$ improves the OER activity (current density at 1.5V) by a factor of eight. The improved OER activity can be directly correlated with the decreased Ir nanoparticle size in the $Ir_{38\%}/W_xTi_{1-x}O_2$. Ir is well dispersed on $W_xTi_{1-x}O_2$ (see **Fig. 5a**), which increases the electrochemical surface area (ECSA) of Ir nanoparticles.

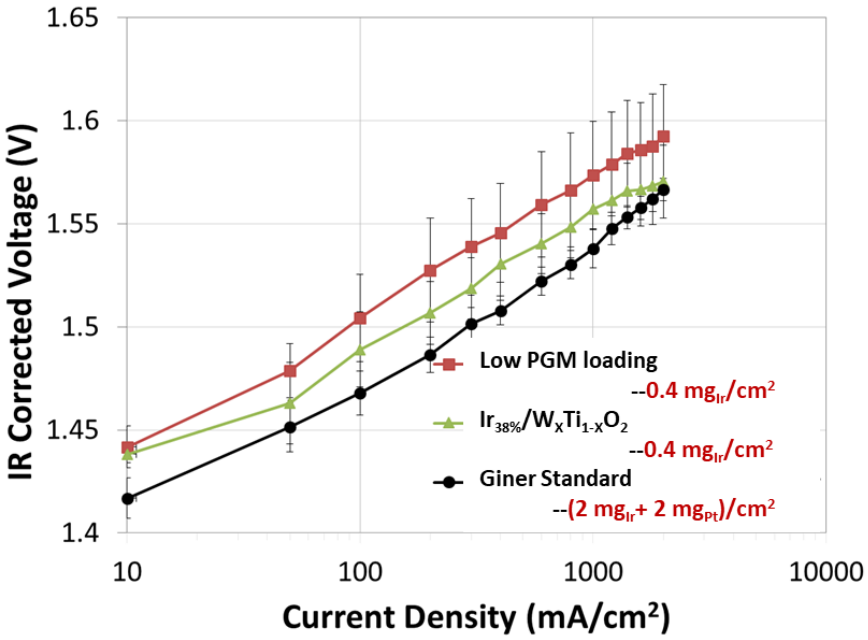

Figure 8. Single cell IR-corrected polarization curves comparing MEAs with low Pt group metal (PGM) loading (0.4 mg_{Ir}/cm^2 - red), $Ir_{38\%}/W\text{-}TiO_2$ (0.4 mg_{Ir}/cm^2 - green), and industry standard Ir-black (2 mg_{Pt}/cm^2+2 mg_{Ir}/cm^2 - black) with Pt/C cathode (0.4 mg_{Pt}/cm^2) at 80 °C.

In addition to initial performance tests, the long-term durability of the same MEA with the $Ir_{38\%}/W_xTi_{1-x}O_2$ anode was investigated (**Fig. 9**). Two approaches were used to explore MEA durability: (1) voltage cycling from 1.4 V to 1.8 V and dwelling time 30 seconds for each voltage. (2) a constant current density test. The MEA incorporating $Ir_{38\%}/W_xTi_{1-x}O_2$ demonstrated remarkable durability; in the voltage-cycling test, the polarization curves after 1500 cycles, 3000 cycles, and 10,000 cycles nearly overlap with the initial curve and no appreciable performance decay was observed. In the constant current density test at 1500 mA/cm^2, slightly less than 20 mV performance degradation was observed after 1200 hours with a steady HFR (0.115 Ohm-cm^2), as shown by the trend line (> 300 hours) in **Fig. 9b**. Transient performance during the initial 300 hours was due to repeated system shutdowns caused by unsteady system operating conditions.

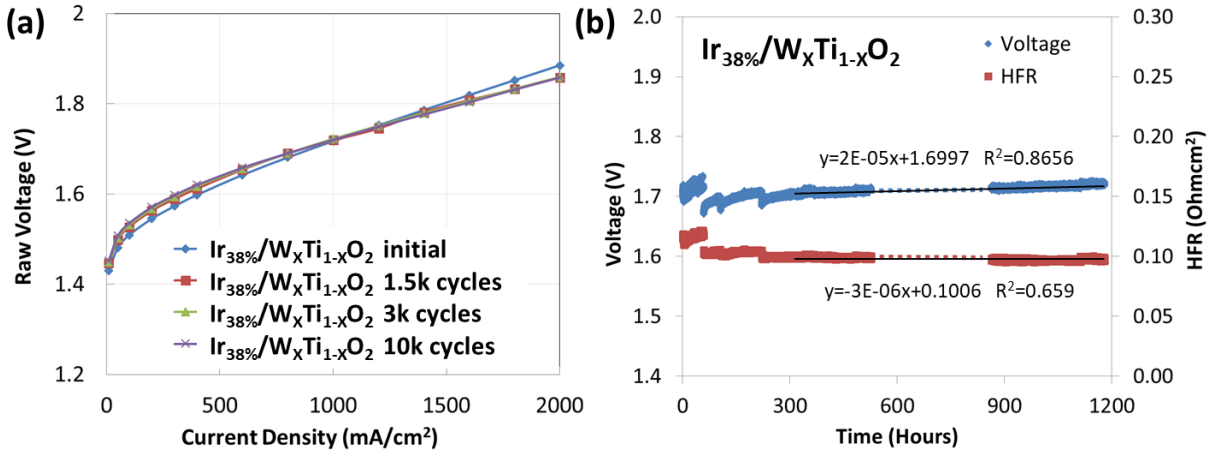

Figure 9. Electrolysis durability of $Ir_{38\%}/W_xTi_{1-x}O_2$ (a) after 10,000 cycles between 1.4-1.8 V (at 0.0167 Hz) in water electrolyzer single cell and (b) at constant current density of 1500 mA/cm^2 for 1200 hours at 80 °C.

To understand the mechanism responsible for the slight activity decay observed during the electrolyzer durability tests, the tested MEAs were analyzed in cross-section using analytical electron microscopy to assess changes in the catalyst layer morphology and elemental distributions. Primary observations of the 15 μm thick anode $Ir_{38\%}/W_xTi_{1-x}O_2$ catalyst layer (**Figs. 10a** and **10b**) after the durability test are the accumulation of Ir at the anode/membrane interface (note that the interface exhibits bright contrast – circled in red in **Figs. 10a** and **10b**) and the oxidation of metallic Ir nanoparticles to form a dense layer of IrO_2 ~0.5 μm thick directly at the interface (**Fig. 10b**, which is a higher magnification of the region within red circle in **Fig. 10a**). In addition, the IrO_2 migrated from the anode side toward the cathode side across the membrane (note bright spots/particles in membrane in **Figs. 10b** and **10c**), and the Ir migration (elemental) profile exhibited a gradient across the membrane, where the amount of IrO_2 was greatest near the anode side, and in fact was highest directly at the interface. **Fig. 10b inset** shows that there is not only oxidation of Ir and migration of IrO_2 from the anode into the membrane, but Pt also migrated from the cathode side across the membrane to the anode side. From the HAADF-STEM images (**Figs. 10a** and **b**) and corresponding EDS map (**Figs. 10c** and **d**), it is clear that the particles within the membrane close to the anode side form "Pt-IrO_2 core-shell" dendritic-shaped particles, where the Pt has migrated from the cathode and the IrO_2 migrates from the anode and preferentially nucleates on the pre-existing Pt particles in the membrane, as shown in **Fig. 10d insert**. Therefore, the slight performance degradation

observed can be attributed to Ir (notably as IrO_2) migration from the anode into the membrane over time during the test. The structural changes and elemental migration did not have a devastating effect on the performance, likely because of the relatively high Ir loading of 0.4 mg_{Ir}/cm^2. New results show that when we further lower the loading to 0.2 or even 0.1 mg_{Ir}/cm^2, the impact of Ir migration and agglomeration on the performance has been manifested.

The $Ir_{38\%}/W_xTi_{1-x}O_2$ catalyst layer microstructural changes before and after the 1200 hour, constant current density test (1500 mA/cm^2) were also characterized by cross-sectional TEM, as shown in **Fig. 11**. The interconnected Ir nanoparticle chain-structure of the $Ir_{38\%}/W_xTi_{1-x}O_2$ catalyst observed in the anode of the fresh MEA (**Fig. 11a**) after decal transfer was very similar to that observed in the $Ir_{38\%}/W_xTi_{1-x}O_2$ catalyst powder, confirming the reason for the consistent activity measured in both RDE and single cell tests (**Fig. 7a**). However, after constant current density testing for 1200 hours, agglomeration of Ir nanoparticles and oxidation of Ir to IrO_2 occurred primarily on the surfaces of pores and at the anode/microporous-layer (MPL) interface (e.g., surface of the anode) after MEA testing (**Figs. 11b** and **11c**) in addition to Ir accumulation at the anode/membrane interface. A similar trend of Ir/IrO_2 migration into the membrane from the anode and Pt migration into the membrane from the cathode was observed after the constant current density test as was observed for the 1.4-1.8 V cycling test.

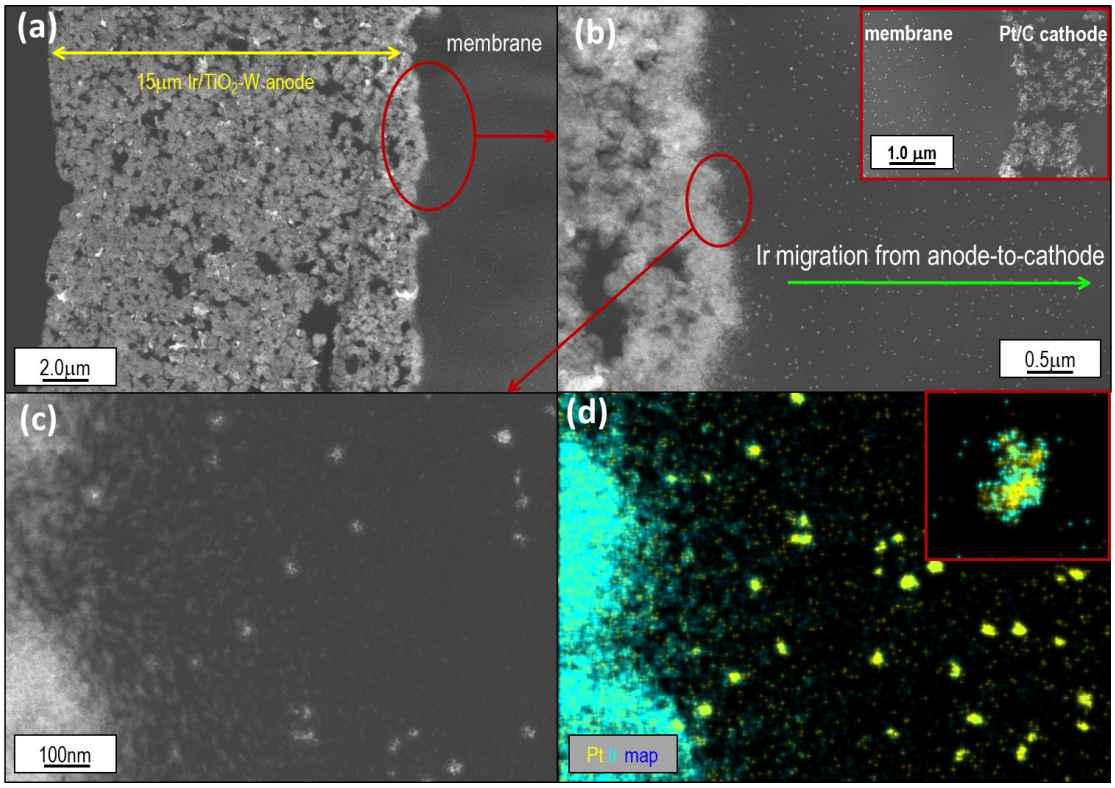

Figure 10. (a) HAADF-STEM image of the post-test MEA with $Ir_{38\%}/W_xTi_{1-x}O_2$ anode after 10,000 cycles between 1.4-1.8 V; (b) HAADF-STEM image of anode/membrane interface at higher magnification from red circled area in (a); inset in (b) is HAADF-STEM image of membrane/cathode (Pt/C) interface; (c) HAADF-STEM image of anode/membrane interface with corresponding (d) EDS elemental map of Pt (yellow) and Ir (green).

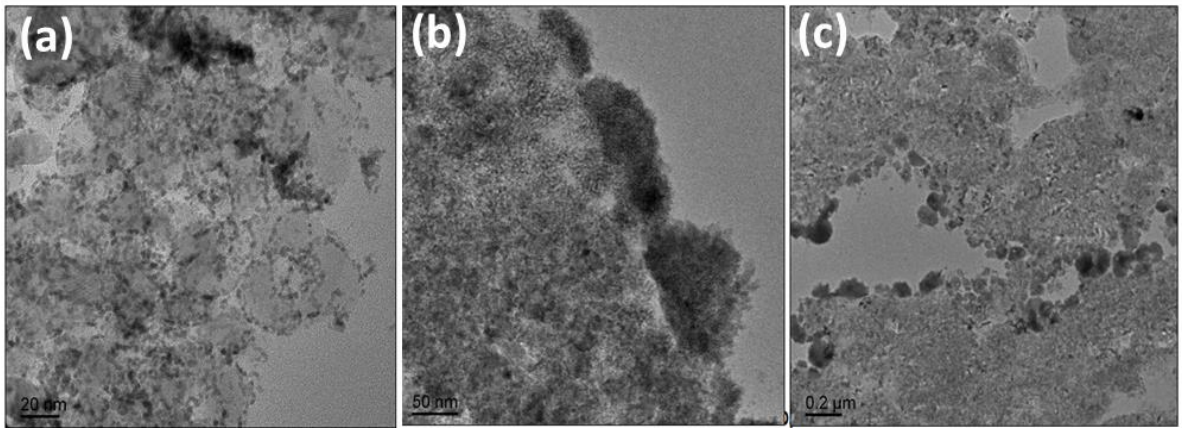

Figure 11. TEM images of (a) fresh MEA with $Ir_{38\%}/W_xTi_{1-x}O_2$ anode layer; (b) TEM image of anode $Ir_{38\%}/W_xTi_{1-x}O_2$ layer surface (adjacent to MPL) showing agglomeration of Ir/IrO_2 and (c) TEM image of highly agglomerated Ir/IrO_2 at pore surfaces of anode $Ir_{38\%}/W_xTi_{1-x}O_2$ layer after durability testing at 1500 mA/cm^2 for 1200 hours at 80 °C**.**

4 Conclusions

In this study, various synthesis parameters were altered to evaluate the template-free and surfactant-free polyol reduction method to disperse Ir nanoparticles on $W_xTi_{1-x}O_2$ supports. The resulting morphologies and effects of the Ir loading were characterized using high-resolution analytical electron microscopy and electrochemical testing. It is concluded that initial electrochemical mass activity for the OER was influenced by the Ir particle size; however, long-term durability was mostly controlled by the Ir loading on the support material. Samples with low Ir loadings tended to expose much more of the $W_xTi_{1-x}O_2$ support surface area after Ir migration and particle coalescence, whereas higher Ir loadings suffered from a significant performance change at initial stage due to the agglomeration of the larger amount of Ir. However, the material with a medium Ir loading, e.g. 38% Ir or $Ir_{38\%}/W_xTi_{1-x}O_2$, exhibited a steady and high mass activity compared to the industry standard, Ir-black, due to its conductive Ir nanoparticle chain-like structure and a high Ir

surface area. For the first time, long-term durability tests were performed using MEAs fabricated with the $Ir_{38\%}/W_xTi_{1-x}O_2$ anode catalyst in the highly oxidizing environment of operating eletrolyzers, with low Ir loading of 0.4 mg/cm^2, and at high current density and voltage. No performance decay was observed during cycling between 1.4 V and 1.8 V for 10,000 cycles. Under even harsher testing conditions (holding the current density at 1500 mA/cm^2 for 1200 hours), less than 20 mV was sacrificed. Therefore, this work provides a good low PGM-loading OER catalyst candidate for industrial application and a synthesis-property-performance relationship discussion for polyol reduction of Ir for future Ir-based OER catalyst design. In addition, a viable, scalable, highly active, and durable low-PGM catalyst is available for the industrial implementation of PEM electrolyzers.

5 Acknowledgements

The project is financially supported by the Department of Energy's Fuel Cell Technology Office under the Grant DE-SC0007471. Microscopy was performed as part of a user project at ORNL's Center for Nanophase Materials Sciences, which is a U.S. Department of Energy, Office of Science User Facility.

6 References

1. Carmo, M., et al., *A comprehensive review on PEM water electrolysis.* International journal of hydrogen energy, 2013. **38**(12): p. 4901-4934.
2. Mallouk, T.E., *Water electrolysis: Divide and conquer.* Nature chemistry, 2013. **5**(5): p. 362-363.

3. Sanchez Casalongue, H.G., et al., *In situ observation of surface species on iridium oxide nanoparticles during the oxygen evolution reaction.* Angewandte Chemie International Edition, 2014. **53**(28): p. 7169-7172.
4. Pfrommer, J., et al., *A Molecular Approach to Self-Supported Cobalt-Substituted ZnO Materials as Remarkably Stable Electrocatalysts for Water Oxidation.* Angewandte Chemie, 2014. **126**(20): p. 5283-5287.
5. Zhao, S., et al., *Determining the Electrochemically Active Area of IrOx Powder Catalysts in an Operating Proton Exchange Membrane Electrolyzer.* ECS Transactions, 2015. **69**(17): p. 877-881.
6. Reier, T., M. Oezaslan, and P. Strasser, *Electrocatalytic oxygen evolution reaction (OER) on Ru, Ir, and Pt catalysts: a comparative study of nanoparticles and bulk materials.* Acs Catalysis, 2012. **2**(8): p. 1765-1772.
7. Zhao, S., et al., *Calculating the Electrochemically Active Surface Area of Iridium Oxide in Operating Proton Exchange Membrane Electrolyzers.* Journal of The Electrochemical Society, 2015. **162**(12): p. F1292-F1298.
8. Huang, K., et al., *Increasing Pt oxygen reduction reaction activity and durability with a carbon-doped TiO 2 nanocoating catalyst support.* Journal of Materials Chemistry, 2012. **22**(33): p. 16824-16832.
9. Huang, K., et al., *Nanoscale conductive niobium oxides made through low temperature phase transformation for electrocatalyst support.* RSC Advances, 2014. **4**(19): p. 9701-9708.
10. Liu, X., X. Wu, and K. Scott, *Study of niobium and tantalum doped titania-supported Pt electrocatalysts for methanol oxidation and oxygen reduction reactions.* Catalysis Science & Technology, 2014. **4**(11): p. 3891-3898.
11. Lewera, A., et al., *Metal–support interactions between nanosized Pt and metal oxides (WO3 and TiO2) studied using X-ray photoelectron spectroscopy.* The Journal of Physical Chemistry C, 2011. **115**(41): p. 20153-20159.
12. Xing, Y., *Synthesis and electrochemical characterization of uniformly-dispersed high loading Pt nanoparticles on sonochemically-treated carbon nanotubes.* The Journal of Physical Chemistry B, 2004. **108**(50): p. 19255-19259.
13. Zhao, S., et al., *Stability and activity of Pt/ITO electrocatalyst for oxygen reduction reaction in alkaline media.* Electrochimica Acta, 2015. **157**: p. 175-182.
14. Roen, L., C. Paik, and T. Jarvi, *Electrocatalytic corrosion of carbon support in PEMFC cathodes.* Electrochemical and Solid-State Letters, 2004. **7**(1): p. A19-A22.
15. Passalacqua, E., et al., *The influence of Pt on the electrooxidation behaviour of carbon in phosphoric acid.* Electrochimica acta, 1992. **37**(15): p. 2725-2730.
16. Kangasniemi, K.H., D. Condit, and T. Jarvi, *Characterization of vulcan electrochemically oxidized under simulated PEM fuel cell conditions.* Journal of The Electrochemical Society, 2004. **151**(4): p. E125-E132.
17. Ferro, S., et al., *On the oxygen evolution reaction at IrO 2-SnO 2 mixed-oxide electrodes.* Electrochimica Acta, 2014. **146**: p. 257-261.
18. Oh, H.-S., et al., *Oxide-supported Ir nanodendrites with high activity and durability for the oxygen evolution reaction in acid PEM water electrolyzers.* Chemical Science, 2015. **6**(6): p. 3321-3328.

19. Nong, H.N., et al., *Oxide-Supported IrNiOx Core–Shell Particles as Efficient, Cost-Effective, and Stable Catalysts for Electrochemical Water Splitting.* Angewandte Chemie International Edition, 2015. **54**(10): p. 2975-2979.
20. Roca-Ayats, M., et al., *Titanium carbide and carbonitride electrocatalyst supports: modifying Pt–Ti interface properties by electrochemical potential cycling.* Journal of Materials Chemistry A, 2014. **2**(44): p. 18786-18790.
21. Zahoor, A., et al., *Carbon/titanium oxide supported bimetallic platinum/iridium nanocomposites as bifunctional electrocatalysts for lithium-air batteries.* Journal of Solid State Electrochemistry, 2016. **20**(5): p. 1397-1404.
22. Zhang, R.-Q., et al., *The role of titanium nitride supports for single-atom platinum-based catalysts in fuel cell technology.* Physical Chemistry Chemical Physics, 2012. **14**(48): p. 16552-16557.
23. Fuerte, A., et al., *Nanosize Ti–W mixed oxides: effect of doping level in the photocatalytic degradation of toluene using sunlight-type excitation.* Journal of Catalysis, 2002. **212**(1): p. 1-9.
24. Fernández-García, M., et al., *Nanostructured Ti− W Mixed-Metal Oxides: Structural and Electronic Properties.* The Journal of Physical Chemistry B, 2005. **109**(13): p. 6075-6083.
25. Guidi, V., et al., *Effect of dopants on grain coalescence and oxygen mobility in nanostructured titania anatase and rutile.* The Journal of Physical Chemistry B, 2003. **107**(1): p. 120-124.
26. Figlarz, M., F. Fievet, and J.-P. Lagier, *Process for the reduction of metallic compounds by polyols, and metallic powders obtained by this process*. 1985, Google Patents.
27. Mezger, J., et al., *Method For Producing Metal Nanoparticles In Polyols*. 2009, Google Patents.
28. Bock, C., et al., *Size-selected synthesis of PtRu nano-catalysts: reaction and size control mechanism.* Journal of the American Chemical Society, 2004. **126**(25): p. 8028-8037.
29. Fuentes, R.E., J. Farell, and J.W. Weidner, *Multimetallic electrocatalysts of Pt, Ru, and Ir supported on anatase and rutile TiO2 for oxygen evolution in an acid environment.* Electrochemical and Solid-State Letters, 2011. **14**(3): p. E5-E7.
30. Wang, Y., et al., *Preparation of tractable platinum, rhodium, and ruthenium nanoclusters with small particle size in organic media.* Chemistry of Materials, 2000. **12**(6): p. 1622-1627.